Computing with Solitons

Darren Rand
Lincoln Laboratory, Massachusetts Institute of Technology
244 Wood Street, Lexington, MA 02420, USA

Ken Steiglitz
Computer Science Department, Princeton University
Princeton, NJ 08544, USA

July 1, 2007

Contents

Glossary

Integrable
This term is generally used in more than one way and in different contexts.

For the purposes of this article, a partial differential equation or system of partial differential equations is *integrable* if it can be solved explicitly to yield *solitons* (qv).

Manakov system
A system of two cubic Schrödinger equations where the self- and cross-phase modulation terms have equal weight.

Nonlinear Schrödinger equation
A partial differential equation that has the same form as the Schrödinger equation of quantum mechanics, with a term nonlinear in the dependent variable, and for the purposes of this article, interpreted classically.

Self- and cross-phase modulation
Any terms in a nonlinear Schrödinger equation that involve nonlinear functions of the dependent variable of the equation, or nonlinear functions of a dependent variable of another (coupled) equation, respectively.

Solitary wave
A solitary wave is a wave characterized by undistorted propagation. Solitary waves do not in general maintain their shape under perturbations or collisions.

Soliton
A soliton is a solitary wave which is also robust under perturbations and collisions.

Turing equivalent
Capable of simulating any Turing Machine, and hence by Turing's Thesis capable of performing any computation that can be carried out by a sequence of effective instructions on a finite amount of data. A machine that is Turing equivalent is therefore as powerful as any digital computer. Sometimes a device that is Turing equivalent is called "universal."

1 Definition of the Subject and Its Importance

Solitons are localized, shape-preserving waves characterized by robust collisions. First observed as a water wave by John Scott Russell (1844) in the Union Canal near Edinburgh and subsequently recreated in the laboratory,

solitons arise in a variety of physical systems, as both temporal pulses which counteract dispersion and spatial beams which counteract diffraction.

Solitons with two components, vector solitons, are computationally universal due to their remarkable collision properties. In this article, we describe in detail the characteristics of Manakov solitons, a specific type of vector soliton, and their applications in computing.

2 Introduction

In this section, we review the basic principles of soliton theory and spotlight relevant experimental results. Interestingly, the phenomena of soliton propagation and collision occur in many physical systems despite the diversity of mechanisms that bring about their existence. For this reason, the discussion in this article will treat temporal and spatial solitons interchangeably, unless otherwise noted.

2.1 Scalar solitons

A pulse in optical fiber undergoes dispersion, or temporal spreading, during propagation. This effect arises because the refractive index of the silica glass is not constant, but is rather a function of frequency. The pulse can be decomposed into a frequency range—the shorter the pulse, the broader its spectral width. The frequency dependence of the refractive index will cause the different frequencies of the pulse to propagate at different velocities, giving rise to dispersion. As a result, the pulse develops a chirp, meaning that the individual frequency components are not evenly distributed throughout the pulse. There are two types of dispersion: normal and anomalous. If the longer wavelengths travel faster, the medium is said to have *normal* dispersion. If the opposite is true, the medium has *anomalous* dispersion.

The response of a dielectric such as optical fiber is nonlinear. Most of the nonlinear effects in fiber originate from nonlinear refraction, where the refractive index n depends on the intensity of the propagating field according to the relation

$$n = n_0 + n_2|E|^2, \tag{1}$$

where n_0 is the linear part of the refractive index, $|E^2|$ is the optical intensity, and n_2 is the coefficient of nonlinear contribution to the refractive index. Because the material responds almost instantaneously, on the order of femtoseconds, and because the phase shift $\Delta\phi$ is proportional to n, each component of an intense optical pulse sees a phase shift proportional to its

intensity. Since the frequency shift $\delta\omega = -(\partial\Delta\phi)/(\partial t)$, the leading edge of the pulse is red-shifted ($\delta\omega < 0$), while the trailing edge is blue-shifted ($\delta\omega > 0$), an effect known as self-phase modulation (SPM). As a result, if the medium exhibits normal dispersion, the pulse is broadened; for anomalous dispersion, the pulse is compressed. Under the proper conditions, this pulse compression can exactly cancel the linear, dispersion-induced broadening, resulting in distortionless soliton propagation. For more details, see the book by Agrawal (2001).

The idealized mathematical model for this pulse propagation is the nonlinear Schrödinger equation (NLSE):

$$i\frac{\partial u}{\partial z} \pm \frac{1}{2}\frac{\partial^2 u}{\partial x^2} + |u|^2 u = 0, \tag{2}$$

where $u(z, x)$ is the complex-valued field envelope, z is a normalized propagation distance and x is normalized time propagating with the group velocity of the pulse. The second and third terms describe dispersion and the intensity-dependent Kerr nonlinearity, respectively. The coefficient of the dispersion term is positive for anomalous dispersion and negative for normal dispersion. Equation (2), known as the *scalar* NLSE, is integrable—that is, it can be solved analytically, and collisions between solitons are 'elastic,' in that no change in amplitude or velocity occurs as a result of a collision. Zakharov and Shabat (1971) first solved this equation analytically using the inverse scattering method. It describes, for example, the propagation of picosecond or longer pulses propagating in optical fiber with anomalous dispersion.

Two solitons at different wavelengths will collide in an optical fiber due to dispersion-induced velocity differences. A schematic of such a collision is depicted in Fig. 1. The scalar soliton collision is characterized by two phenomena—a position and phase shift—both of which can be understood in the same intuitive way. During collision, there will be a local increase in intensity, causing a local increase in the fiber's refractive index, according to Eq. (1). As a result, both the soliton velocity and phase will be affected during the collision.

From an all-optical signal processing perspective, the phase and position shifts in a soliton collision are not useful. This is because these effects are independent of any soliton properties that are changed by collision; that is, the result of one collision will not affect the result of subsequent collisions. Scalar solitons are therefore not useful for complex logic or computing, which depend on multiple, cascaded interactions.

Despite this setback, it was discovered later that a system similar to the scalar NLSE, the Manakov system (Manakov, 1973), possesses very

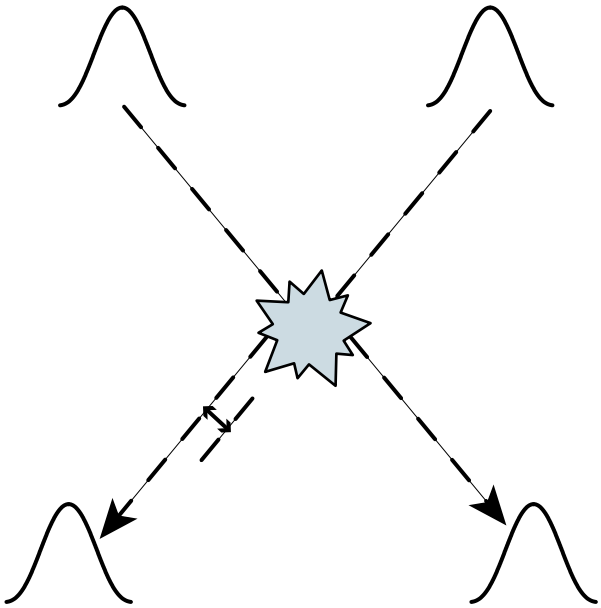

Figure 1: Schematic of a scalar soliton collision, in which amplitude and velocities are unchanged. The two soliton collision effects are a position shift (depicted through the translational shift in the soliton path) and phase shift (not pictured).

rich collisional properties (Radhakrishnan et al., 1997) and is integrable as well. Manakov solitons are a specific instance of two-component vector solitons, and it has been shown that collisions of Manakov solitons are capable of transferring information via changes in a complex-valued polarization state (Jakubowski et al., 1998).

2.2 Vector solitons

When several field components, distinguished by polarization and/or frequency, propagate in a nonlinear medium, the nonlinear interaction between them must be considered as well. This interaction between field components results in intensity-dependent nonlinear coupling terms analogous to the self-phase modulation term in the scalar case. Such a situation gives rise to a set of coupled nonlinear Schrödinger equations, and may allow for propagation of *vector* solitons. For the case of two components propagating in an ideal lossless medium with no higher-order effects and only intensity-dependent nonlinear coupling, the equations become:

$$\begin{aligned} i\frac{\partial u_1}{\partial z} + \frac{\partial^2 u_1}{\partial x^2} + 2\mu(|u_1|^2 + \alpha|u_2|^2)u_1 = 0, \\ i\frac{\partial u_2}{\partial z} + \frac{\partial^2 u_2}{\partial x^2} + 2\mu(|u_2|^2 + \alpha|u_1|^2)u_2 = 0, \end{aligned} \tag{3}$$

where $u_1(z,x)$ and $u_2(z,x)$ are the complex-valued pulse envelopes for each component, μ is a nonlinearity parameter, and α describes the ratio between self- and cross-phase modulation contributions to the overall nonlinearity. Only for the special case of $\alpha = 1$ are Eqs. 3 integrable. First solved using the method of inverse scattering by Manakov (1973), Eqs. 3 admit solutions known as Manakov solitons. For nonintegrable cases ($\alpha \neq 1$), some analytical solitary-wave solutions are known for specific cases, although in general a numerical approach is required (Yang, 1997). The specific case of $\alpha = 2/3$, for example, corresponds to linearly birefringent polarization maintaining fiber, and will be considered in more detail in Section 6.

Due to their multicomponent structure, vector solitons have far richer collision dynamics than their scalar, one-component counterparts. Recall that scalar solitons are characterized by phase and position shifts only. Vector soliton collisions also exhibit these effects, with the added feature of possible intensity redistributions between the component fields (Manakov, 1973; Radhakrishnan et al., 1997). This process is shown schematically in Fig. 2. In the collision, two conservation relations are satisfied: (i) the energy in each soliton is conserved and (ii) the energy in each component

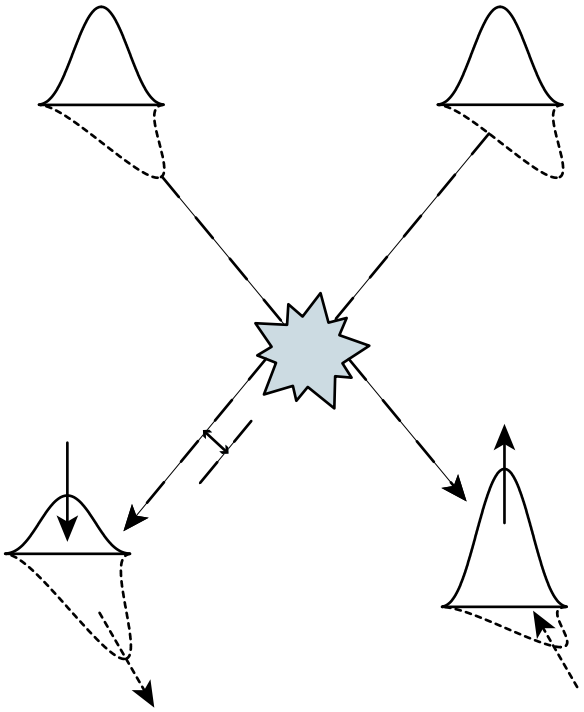

Figure 2: Schematic of a vector soliton collision, which exhibits a position shift and phase shift (not pictured), similar to the scalar soliton collision (cf. Fig. 1). Vector soliton collisions also display an energy redistribution among the component fields, shown here as two orthogonal polarizations. Arrows indicate direction of energy redistribution.

is conserved. It can be seen that when the amplitude of one component in a soliton increases as a result of the collision, the other component decreases, with the opposite exchange in the second soliton. The experimental observation of this effect will be discussed in Section 6. In addition to fundamental interest in such solitons, collisions of vector solitons make possible unique applications, including collision-based logic and universal computation (Jakubowski et al., 1998; Steiglitz, 2000; Steiglitz, 2001; Rand et al., 2005), as discussed in Section 4.

3 Manakov solitons

As mentioned in Section 2, computation is possible using vector solitons because of an energy redistribution that occurs in a collision. In this section, we provide the mathematic background of Manakov soliton theory, in order to understand soliton computing and a remarkable way to achieve bistability using soliton collisions as described in Sections 4 and 5, respectively.

The Manakov system consists of two coupled NLSEs (Manakov, 1973):

$$\begin{aligned} i\frac{\partial q_1}{\partial z} + \frac{\partial^2 q_1}{\partial x^2} + 2\mu(|q_1|^2 + |q_2|^2)q_1 = 0, \\ i\frac{\partial q_2}{\partial z} + \frac{\partial^2 q_2}{\partial x^2} + 2\mu(|q_1|^2 + |q_2|^2)q_2 = 0, \end{aligned} \tag{4}$$

where $q_1(x, z)$ and $q_2(x, z)$ are two interacting optical components, μ is a positive parameter representing the strength of the nonlinearity, and x and z are normalized space and propagation distance, respectively. As mentioned in Section 2.2, the Manakov system is a special case of Eq. (3) with $\alpha = 1$. The two components can be thought of as components in two polarizations, or, as in the case of a photorefractive crystal, two uncorrelated beams (Christodoulides et al., 1996).

Manakov first solved Eqs. (4) by the method of inverse scattering (1973). The system admits single-soliton, two-component solutions that can be characterized by a complex number $k \equiv k_R + ik_I$, where k_R represents the energy of the soliton and k_I the velocity, all in normalized units. The additional soliton parameter is the complex-valued polarization state $\rho \equiv q_1/q_2$, defined as the (z- and x- independent) ratio between the q_1 and q_2 components.

Figure 3 shows the schematic for a general two-soliton collision, with initial parameters ρ_1, k_1 and ρ_L, k_2, corresponding to the right-moving and left-moving solitons, respectively. The values of k_1 and k_2 remain constant during collision, but in general the polarization state changes. Let ρ_1 and

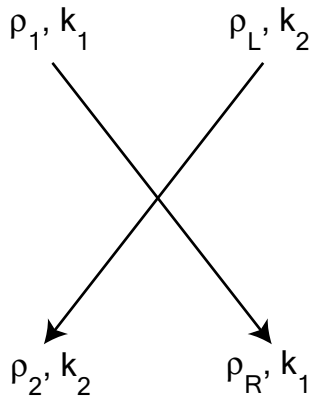

Figure 3: Schematic of a general two-soliton collision. Each soliton is characterized by a complex-valued polarization state ρ and complex parameter k. Reprinted with permission from (Steiglitz, 2000). Copyright by the American Physical Society.

ρ_L denote the respective soliton states before impact, and suppose the collision transforms ρ_1 into ρ_R, and ρ_L into ρ_2. It turns out that the state change undergone by each colliding soliton takes on the very simple form of a linear fractional transformation (also called a bilinear or Möbius transformation). Explicitly, the state of the emerging left-moving soliton is given by (Jakubowski et al., 1998):

$$\rho_2 = \frac{[(1-g)/\rho_1^* + \rho_1]\rho_L + g\rho_1/\rho_1^*}{g\rho_L + (1-g)\rho_1 + 1/\rho_1^*}, \tag{5}$$

where

$$g \equiv \frac{k_1 + k_1^*}{k_2 + k_1^*}. \tag{6}$$

The state of the right-moving soliton is obtained similarly, and is

$$\rho_R = \frac{[(1-h^*)/\rho_L^* + \rho_L]\rho_1 + h^*\rho_L/\rho_L^*}{h^*\rho_1 + (1-h^*)\rho_L + 1/\rho_L^*}, \tag{7}$$

where

$$h \equiv \frac{k_2 + k_2^*}{k_1 + k_2^*}. \tag{8}$$

We assume here, without loss of generality, that $k_{1R}, k_{2R} > 0$.

Several properties of the linear fractional transformations in Eqs. (5) and (7) are derived in (Jakubowski et al., 1998), including the characterization

of inverse operators, fixed points, and implicit forms. In particular, when viewed as an operator every soliton has an *inverse*, which will undo the effect of the operator on the state. Note that this requires that the inverse operator have the same k parameter as the original, a condition that will hold in our application of computing in the next section.

These state transformations were first used by Jakubowski et al. (1998) to describe logical operations such as NOT. Later, Steiglitz (2000) established that arbitrary computation was possible through time gating of Manakov (1+1)-dimensional spatial solitons. We will describe this in section 4.

There exist several candidates for the physical realization of Manakov solitons, including photorefractive crystals (Christodoulides et al., 1996; Shih and Segev, 1996; Chen et al., 1996; Anastassiou et al., 1999; Anastassiou et al., 2001), semiconductor waveguides (Kang et al., 1996), quadratic media (Steblina et al., 2000), and optical fiber (Menyuk, 1989; Rand et al., 2007). In Section 6, we discuss in detail an experiment with vector solitons in linearly birefringent optical fiber.

4 Manakov soliton computing

We described in the previous section how collisions of bright Manakov solitons can be described by transformations of a complex-valued state which is the ratio between the two Manakov components. We show in this section that general computation is possible if we use (1+1)-dimensional spatial solitons that are governed by the Manakov equations and if we are allowed to time-gate the beams input to the medium. The result is a dynamic computer without spatially fixed gates or wires, which is unlike most present-day conceptions of a computer that involve integrated circuits, in which information travels between logical elements that are fixed spatially through fabrication on a silicon wafer. We can call such a scheme "nonlithographic," in the sense that there is no architecture imprinted on the medium.

The requirements for computation include cascadability, fanout, and Boolean completeness. The first, cascadability, requires that the output of one device can serve as input to another. Since any useful computation consists of many stages of logic, this condition is essential. The second, fanout, refers to the ability of a logic gate to drive at least two similar gates. Finally, Boolean completeness makes it possible to perform arbitrary computation.

We should emphasize that although the model we use is meant to reflect known physical phenomena, at least in the limit of ideal behavior, the result is a mathematical one. Practical considerations of size and speed are not

considered here, nor are questions of error propagation. In this sense the program of this article is analogous to Fredkin and Toffoli (1982) for ideal billiard balls, and Shor (1994) for quantum mechanics. There are however several candidates for physical instantiation of the basic ideas in this paper, as noted in the previous section.

Although we are describing computation embedded in a homogeneous medium, and not interconnected *gates* in the usual sense of the word, we will nevertheless use the term *gates* to describe prearranged sequences of soliton collisions that effect logical operations. We will in fact adopt other computer terms to our purpose, such as *wiring* to represent the means of moving information from one place to another, and *memory* to store it in certain ways for future use.

We will proceed in the construction of what amounts to a complete computer in the following stages: First we will describe a basic gate that can be used for FANOUT. Then we will show how the same basic configuration can be used for NOT, and finally, NAND. Then we will describe ways to use time gating of the input beams to interconnect signals. The NAND gate, FANOUT, and interconnect are sufficient to implement any computer, and we conclude with a layout scheme for a general-purpose, and hence Turing-equivalent computer. The general picture of the physical arrangement is shown in Fig. 4.

Figure 5 shows the usual picture of colliding solitons, which can work interchangeably for the case of temporal or spatial solitons. It is convenient for visualization purposes to turn the picture and adjust the scale so the axes are horizontal and vertical, as in Fig. 6. We will use binary logic, with two distinguished, distinct complex numbers representing TRUE and FALSE, called 1 and 0, respectively. In fact, it turns out to be possible to use complex 1 and 0 for these two state values, and we will do that throughout this paper, but this is a convenience and not at all a necessity. We will thus use complex polarization states 1 and 0 and logical 1 and 0 interchangeably.

4.1 FANOUT

We construct the FANOUT gate by starting with a COPY gate, implemented with collisions between three down-moving, vertical solitons and one left-moving horizontal soliton. Figure 7 shows the arrangement. The soliton state labeled *in* will carry a logical value, and so be in one of the two states 0 or 1. The left-moving soliton labeled *actuator* will be in the fixed state 0, as will be the case throughout this paper. The plan is to adjust the (so far) arbitrary states z and y so that $out = in$, justifying the name COPY. It

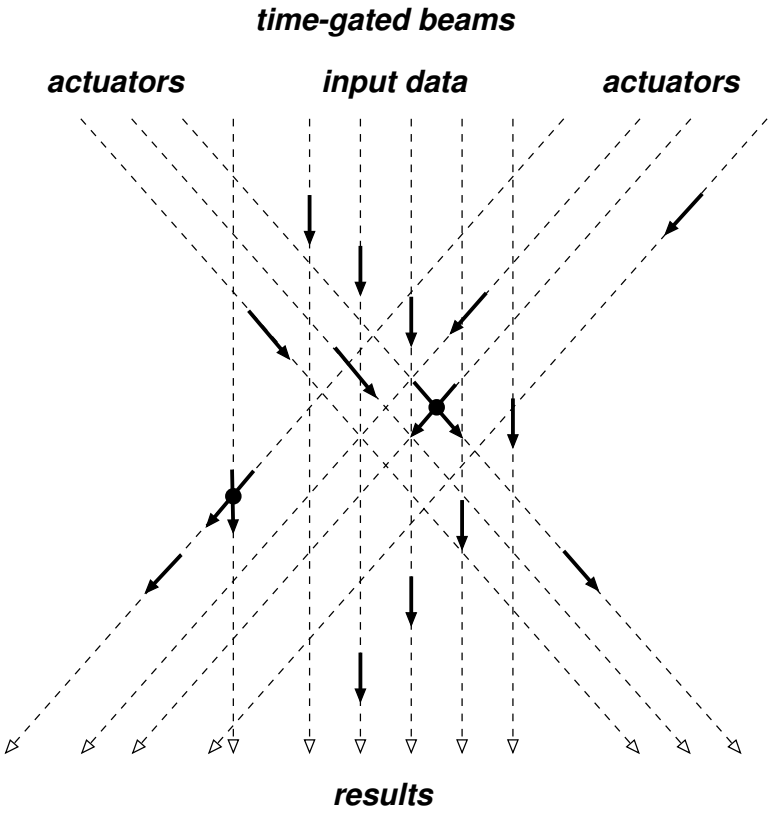

Figure 4: The general physical arrangement considered in this paper. Time-gated beams of spatial Manakov solitons enter at the top of the medium, and their collisions result in state changes that reflect computation. Each solid arrow represents a beam segment in a particular state. Reprinted with permission from (Steiglitz, 2000). Copyright by the American Physical Society.

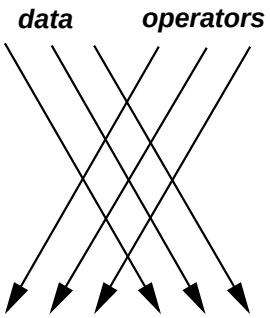

Figure 5: Colliding spatial solitons. Reprinted with permission from (Steiglitz, 2000). Copyright by the American Physical Society.

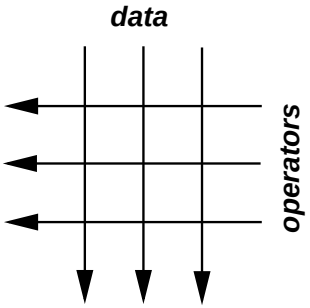

Figure 6: Convenient representation of colliding spatial solitons. Reprinted with permission from (Steiglitz, 2000). Copyright by the American Physical Society.

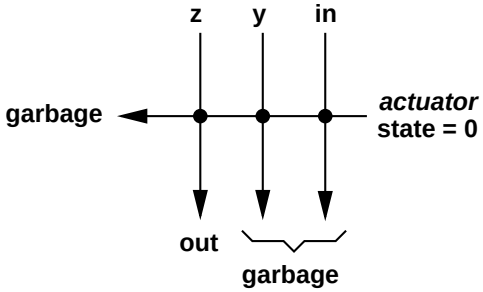

Figure 7: COPY gate. Reprinted with permission from (Steiglitz, 2000). Copyright by the American Physical Society.

Table 1: Parameters for gates when soliton speeds are 1.

gate	z	y
COPY	$-0.24896731 - 0.62158212 \cdot \mathrm{I}$	$2.28774210 + 0.01318152 \cdot \mathrm{I}$
NOT	$-0.17620885 + 0.38170630 \cdot \mathrm{I}$	$0.07888703 - 1.26450654 \cdot \mathrm{I}$
ONE	$-0.45501471 - 1.37634227 \cdot \mathrm{I}$	$1.43987094 + 0.64061349 \cdot \mathrm{I}$
Z-CONV	$0.31838068 - 0.43078735 \cdot \mathrm{I}$	$-0.04232340 + 2.17536612 \cdot \mathrm{I}$
Y-CONV	$1.37286955 + 0.88495501 \cdot \mathrm{I}$	$-0.58835758 - 0.18026939 \cdot \mathrm{I}$

is reasonable to expect that this might be possible, because there are four degrees of freedom in the two complex numbers z and y, and two complex equations to satisfy: that *out* be 1 and 0 when *in* is 1 and 0, respectively. Values that satisfy these four equations in four unknowns were obtained numerically. We will call them z_c and y_c. It is not always possible to solve these equations; Ablowitz et al (2004) showed that a unique solution is guaranteed to exist in certain parameter regimes. However, explicit solutions have been found for all the cases used in this section, and are given in Table 4.1.

To be more specific about the design problem, write Eq. (5) as the left-moving product $\rho_2 = L(\rho_1, \rho_L)$, and similarly write Eq. (7) as $\rho_R = R(\rho_1, \rho_L)$. The successive left-moving products in Fig. 7 are $L(in, 0)$ and $L(y, L(in, 0))$. The *out* state is then $R(z, L(y, L(in, 0))$. The stipulation that 0 maps to 0 and 1 maps to 1 is expressed by the following two simultaneous complex equations in two complex unknowns

$$\begin{aligned} R(z, L(y, L(0, 0)) &= 0, \\ R(z, L(y, L(1, 0)) &= 1. \end{aligned} \tag{9}$$

It is possible to solve for z as a function of y and then eliminate z from the equations, yielding one complex equation in the one complex unknown y. This is then solved numerically by grid search and successive refinement. There is no need for efficiency here, since we will require solutions in only a small number of cases.

To make a FANOUT gate, we need to recover the input, which we can do using a collision with a soliton in the state which is the inverse of 0, namely ∞ (Jakubowski et al., 1998). Figure 8 shows the complete FANOUT gate. Notice that we indicate collisions with a dot at the intersection of paths, and require that the continuation of the inverse soliton not intersect the continuation of z that it meets. We indicate that by a broken line,

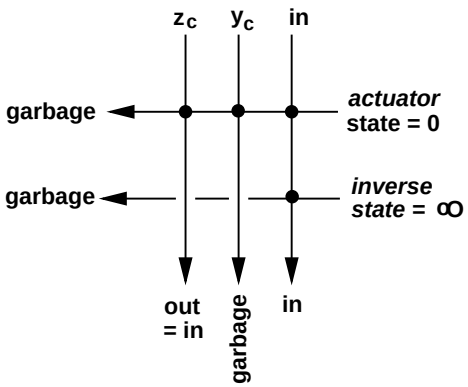

Figure 8: FANOUT gate. Reprinted with permission from (Steiglitz, 2000). Copyright by the American Physical Society.

and postpone the explanation of how this "wire crossing" is accomplished. It is immaterial whether the continuation of the inverse operator hits the continuation of y, because it is not used later. We call such solitons *garbage* solitons.

4.2 NOT and ONE gates

In the same way we designed the complex pair of states (z_c, y_c) to produce a COPY and FANOUT gate, we can find a pair (z_n, y_n) to get a NOT gate, mapping 0 to 1 and 1 to 0; and a pair (z_1, y_1) to get a ONE gate, mapping both 0 and 1 to 1. These (z, y) values are given in Table 4.1.

We should point out that the ONE gate in itself, considered as a one-input, one-output gate, is not invertible, and could never be achieved by using the continuation of one particular soliton through one, or even many collisions. This is because such transformations are always nonsingular linear fractional transformations, which are invertible (Jakubowski et al., 1998). The transformation of state from the input to the continuation of z is, however, much more complicated and provides the flexibility we need to get the ONE gate. It turns out that this ONE gate will give us a row in the truth table of a NAND, and is critical for realizing general logic.

4.3 Output/input converters, two-input gates, and NAND

To perform logic of any generality we must of course be able to use the output of one operation as the input to another. To do this we need to convert logic

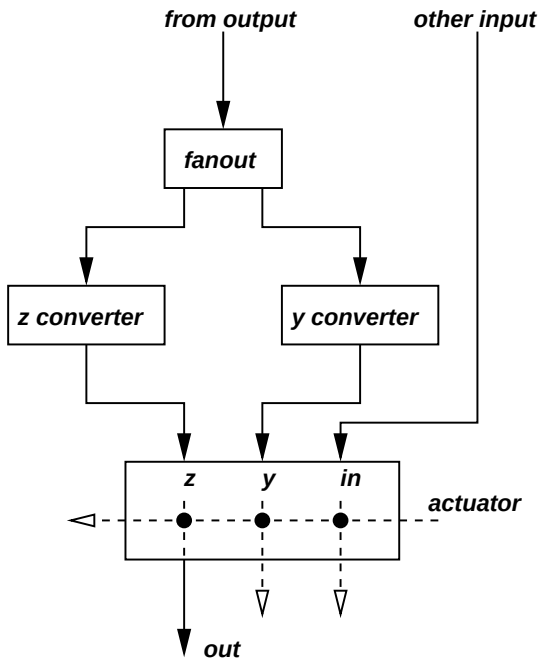

Figure 9: A NAND gate, using converter gates to couple copies of one of its inputs to its z and y parameters. Reprinted with permission from (Steiglitz, 2000). Copyright by the American Physical Society.

(0/1) values to some predetermined z and y values, the choice depending on the type of gate we want. This results in a two-input, one-output gate.

As an important example, here's how a NAND gate can be constructed. We design a z-converter that converts 0/1 values to appropriate values of z, using the basic three-collision arrangement shown in Fig. 7. For a NAND gate, we map 0 to z_1, the z value for the ONE gate, and map 1 to z_n, the z value for the NOT gate. Similarly, we construct a y-converter that maps 0 to y_1 and 1 to y_n. These z- and y-converters are used on the fanout of one of the inputs, and the resulting two-input gate is shown in Fig. 9. Of course these z- and y-converters require z and y values themselves, which are again determined by numerical search (see Table 4.1).

The net effect is that when the left input is 0, the other input is mapped by a ONE gate, and when it is 1 the other input is mapped by a NOT gate. The only way the output can be 0 is if both inputs are 1, thus showing that this is a NAND gate. Another way of looking at this construction is that the 2×2 truth table of (left input)×(right input) has as its 0 row a ONE gate of

the columns (1 1), and as its 1 row a NOT gate of the columns (1 0).

The importance of the NAND gate is that it is *universal* (Mano, 1972). That is, it can be used with interconnects and fanouts to construct any other logical function. Thus we have shown that with the ability to "wire" we can implement any logic using the Manakov model.

We note that other choices of input converters result in direct realizations of other gates. Using input converters that convert 0 and 1 to (z_c, y_c) and (z_n, y_n), respectively, results in a truth table with first row (0 1) and second row (1 0), an XOR gate. Converting 0 and 1 to (z_c, y_c) and (z_1, y_1), respectively, results in an OR gate, and so on.

4.4 Time gating

We next take up the question of interconnecting the gates described above, and begin by showing how the continuation of the input in the COPY gate can be restored without affecting the other signals. In other words, we show how a simple "wire crossing" can be accomplished in this case.

For spatial solitons, the key flexibility in the model is provided by assuming that input beams can be time-gated; that is, turned on and off. When a beam is thus gated, a finite segment of light is created that travels through the medium. We can think of these finite segments as finite light pulses, and we will call them simply *pulses* in the remainder of this paper.

Figure 10(a) shows the basic three-collision gate implemented with pulses. Assuming that the actuator and data pulses are appropriately timed, the actuator pulse hits all three data pulses, as indicated in the projection below the space-space diagram. The problem is that if we want a later actuator pulse to hit the rightmost data pulse (to invert the state, for example, as in the FANOUT gate), it will also hit the remaining two data pulses because of the way they must be spaced for the earlier three collisions.

We can overcome this difficulty by sending the actuator pulse from the left instead of the right. Timing it appropriately early it can be made to miss the first two data pulses, and hit the third, as shown in Fig. 10(b). It is easy to check that if the velocity of the right-moving actuator solitons is algebraically above that of the data solitons by the same amount that the velocity of the data solitons is algebraically above that of the left-moving actuator solitons, the same state transformations will result. For example, if we choose the velocities of the data and left-moving actuator solitons to be $+1$ and -1, we should choose the velocity of the right-moving actuator solitons to be $+3$. This is really a consequence of the fact that the g and h parameters of Eqs. (6) and (8) in the linear fractional transformation depend

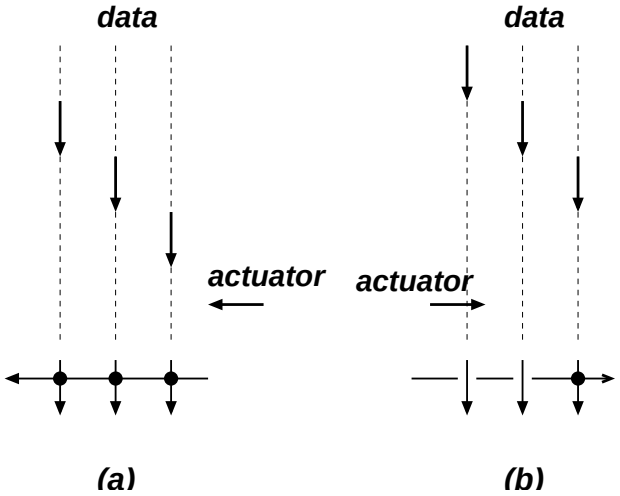

Figure 10: (a) When entered from the right and properly timed, the actuator pulse hits all three data pulses, as indicated in the projection at the bottom; (b) When entered from the left and properly timed, the actuator pulse misses two data pulses and hits only the rightmost data pulse, as indicated in the projection at the bottom. Reprinted with permission from (Steiglitz, 2000). Copyright by the American Physical Society.

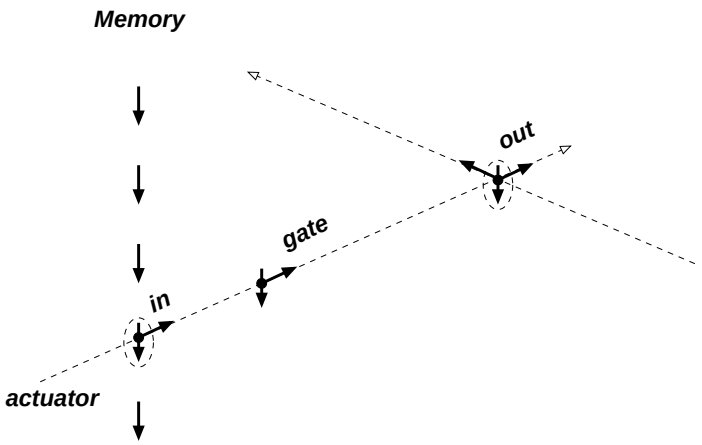

Figure 11: The frame of this figure is moving down with the data pulses on the left. A data pulse in memory is operated on with a three-collision gate actuated from the left, and the result deposited to the upper right. Reprinted with permission from (Steiglitz, 2000). Copyright by the American Physical Society.

only on the difference in the velocities of the colliding solitons.

4.5 Wiring

Having shown that we can perform FANOUT and NAND, it remains only to show that we can "wire" gates so that any outputs can be fed to any inputs. The basic method for doing this is illustrated in Fig. 11. We think of data as stored in the down-moving pulses in a column, which we can think of as "memory". The observer moves with this frame, so the data appears stationary.

Pulses that are horizontal in the three-collision gates shown in previous figures will then appear to the observer to move upward at inclined angles. It is important to notice that these upward diagonally moving pulses are evanescent in our picture (and hence their paths are shown dashed in the figure). That is, once they are used, they do not remain in the picture with a moving frame and hence cannot interfere with later computations. However, all vertically moving pulses remain stationary in this picture.

Once a diagonal trajectory is used for a three-collision gate, reusing it will in general corrupt the states of all the stationary pulses along that diagonal. However, the original data pulse (gate input) can be restored with a pulse

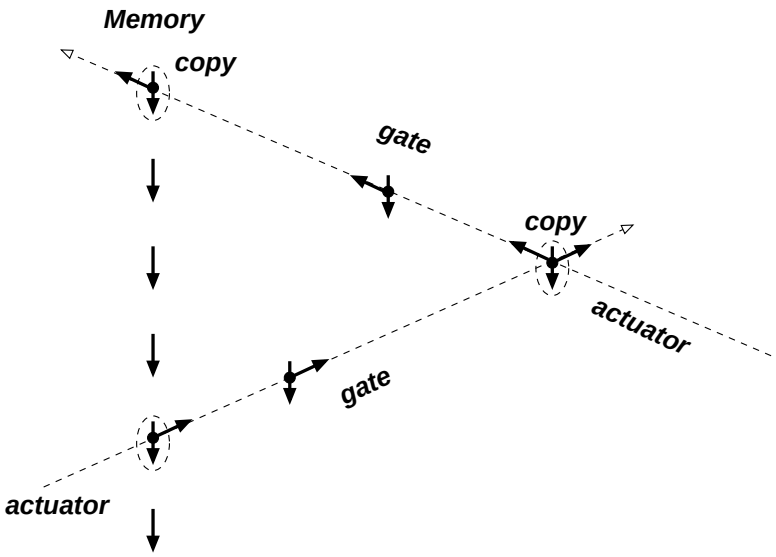

Figure 12: A data pulse is copied to the upper right, this copy is copied to the upper left, and the result put at the top of memory. The original data pulse can then be restored with an inverse pulse and copied to the left in the same way. Reprinted with permission from (Steiglitz, 2000). Copyright by the American Physical Society.

in the state inverse to the actuator, either along the same diagonal as the actuator, provided we allow enough time for the result (the gate output, a stationary z pulse) to be used, or along the other diagonal.

Suppose we want to start with a given data pulse in the memory column and create two copies above it in the memory column. Figure 12 shows a data pulse at the lower left being copied to the upper right with a three-collision COPY gate, initiated with an actuator pulse from the left. This copy is then copied again to the upper left, back to a waiting z pulse in the memory column. After the first copy is used, an inverse pulse can be used along the lower left to upper right diagonal to restore the original data pulse. The restored data pulse can then be copied to the left in the same way, to a height above the first copy, say, and thus two copies can be created and deposited in memory above the original.

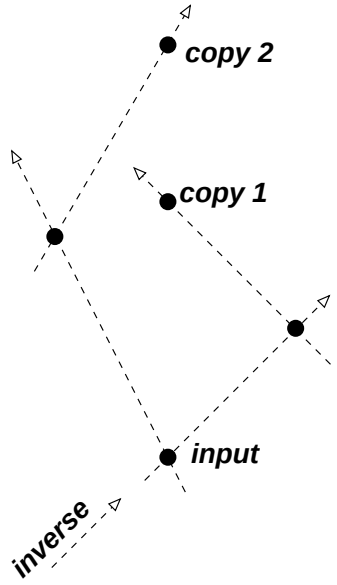

Figure 13: The introduction of a second speed makes true FANOUT possible. For simplicity, in this and the next figure, data and operator pulses are indicated by solid dots, and the y operator pulses are not shown. The paths of actuator pulses are indicated by dashed lines. Reprinted with permission from (Steiglitz, 2000). Copyright by the American Physical Society.

4.6 A second speed and final FANOUT and NAND

There is one problem still remaining with a true FANOUT: When an original data pulse in memory is used in a COPY operation for FANOUT, two diagonals are available, one from the lower left to the upper right, and the other from the lower right to the upper left. Thus, two copies can be made, as was just illustrated. However, when a data pulse is deposited in the memory column as a result of a logic operation, the logical operation itself uses at least one diagonal, which leaves at most one free. This makes a FANOUT of the *output* of a gate impossible with the current scheme.

A simple solution to this problem is to introduce another speed, using velocities ± 0.5, say, in addition to ± 1. This effectively provides four rather than two directions in which a pulse can be operated on, and allows true FANOUT and general interconnections. Figure 13 shows such a FANOUT; the data pulse at the lower left is copied to a position above it using one speed, and to another position, above that, using another.

Finally, a complete NAND gate is shown in Fig. 14. The gate can be

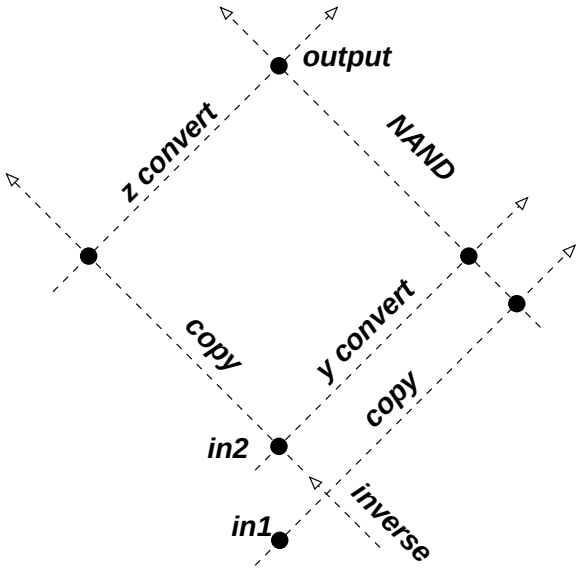

Figure 14: Implementation of a NAND gate. A second speed will be necessary to use the output. Reprinted with permission from (Steiglitz, 2000). Copyright by the American Physical Society.

thought of as composed of the following steps:

- input 2 is copied to the upper left, and that copy transformed by a z-converter to the upper right, placing the z pulse for the NAND gate at the top of the figure;
- after the copy of input 2 is used, input 2 is restored with an inverse pulse to the upper left;
- input 2 is then transformed to the upper right by a y-converter;
- input 1 is copied to the upper right, to a position collinear with the z- and y-converted versions of the other input;
- a final actuator pulse converts the z pulse at the top to the output of the NAND gate.

Note that the output of the NAND has used two diagonals, which again shows why a second speed is needed if we are to use the NAND output as an input to subsequent logical operations. The y operator pulses, middle components in the three-collision COPY and converter gates, are not shown

in the figure, but room can always be made for them to avoid accidental collisions by adding only a constant amount of space.

4.7 Universality

It should be clear now that any sequence of three-collision gates can be implemented in this way, copying data out of the memory column to the upper left or right, and performing NAND operations on any two at a time in the way shown in the previous section. The computation can proceed in a breadth-first manner, with the results of each successive stage being stored above the earlier results. Each additional gate can add only a constant amount of height and width to the medium, so the total area required is no more than proportional to the square of the number of gates.

The "program" consists of down-moving y and z operator pulses, entering at the top with the down-moving data, and actuator pulses that enter from the left or right at two different speeds. In the frame moving with the data, the data and operator pulses are stationary and new results are deposited at the top of the memory column. In the laboratory frame the data pulses leave the medium downward, and new results appear in the medium at positions above the old data, at the positions of newly entering z pulses.

4.8 Discussion

We have shown that in principle any computation can be performed by shining time-gated lasers into a completely homogeneous nonlinear optical medium. This result should be viewed as mathematical, and whether the physics of vector soliton collisions can lead to practical computational devices is a subject for future study. With regard to the economy of the model, the question of whether time gating is necessary, or even whether two speeds are necessary, is open.

We note that the result described here differs from the universality results for the ideal billiard ball model (Fredkin and Toffoli, 1982), the Game of Life (Berlekamp et al., 1982), and Lattice Gasses (Squier and Steiglitz, 1993), for example, in that no internal mirrors or structures of any kind are used inside the medium. To the author's knowledge, whether internal structure is necessary in these other cases is open.

Finally, we remark that the model used is reversible and dissipationless. The fact that some of the gate operations realized are not in themselves reversible is not a contradiction, since extra, "garbage" solitons (Fredkin and Toffoli, 1982) are produced that save enough state to run the computation

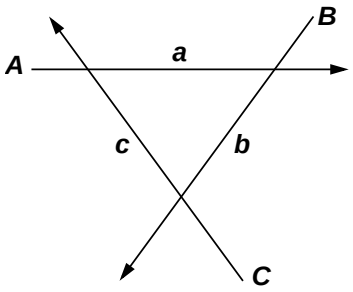

Figure 15: The basic cycle of three collisions. Reprinted with permission from (Steiglitz, 2001). Copyright by the American Physical Society.

backwards.

5 Multistable soliton collision cycles

Bistable and multistable optical systems, besides being of some theoretical interest, are of practical importance in offering a natural "flip-flop" for noise immune storage and logic. We show in this section that simple cycles of collisions of solitons governed by the Manakov equations can have more than one distinct stable set of polarization states, and therefore these distinct equilibria can, in theory, be used to store and process information. The multistability occurs in the polarization states of the beams; the solitons themselves do not change shape and remain the usual sech-shaped solutions of the Manakov equations. This phenomenon is dependent only on simple soliton collisions in a completely homogeneous medium.

The basic configuration considered requires only that the beams form a closed cycle, and can thus be realized in any nonlinear optical medium that supports spatial Manakov solitons. The possibility of using multistable systems of beam collisions broadens the possibilities for practical application of the surprisingly strong interactions that Manakov solitons can exhibit, a phenomenon originally described in (Radhakrishnan et al., 1997). We show here by example that a cycle of three collisions can have two distinct foci surrounded by basins of attractions, and that a cycle of four collisions can have three.

5.1 The basic three-cycle and computational experiments

Figure 15 shows the simplest example of the basic scheme, a cycle of three beams, entering in states A, B, and C, with intermediate beams a, b, and

c. For convenience, we will refer to the beams themselves, as well as their states, as A, B, C, etc. Suppose we start with beam C initially turned off, so that $A = a$. Beam a then hits B, thereby transforming it to state b. If beam C is then turned on, it will hit A, closing the cycle. Beam a is then changed, changing b, etc., and the cycle of state changes propagates clockwise. The question we ask is whether this cycle converges, and if so, whether it will converge with any particular choice of complex parameters to exactly zero, one, two, or more foci. We answer the question with numerical simulations of this cycle.

A typical computational experiment was designed by fixing the input beams A, B, C, and the parameters k_1 and k_2, and then choosing points a randomly and independently with real and imaginary coordinates uniformly distributed in squares of a given size in the complex plane. The cycle described above was then carried out until convergence in the complex numbers a, b, and c was obtained to within 10^{-12} in norm. Distinct foci of convergence were stored and the initial starting points a were categorized by which focus they converged to, thus generating the usual picture of basins of attraction for the parameter a. Typically this was done for 50,000 random initial values of a, effectively filling in the square, for a variety of parameter choices A, B, and C. The following results were observed:

- In cases with one or two clear foci, convergence was obtained in every iteration, almost always within one or two hundred iterations.
- Each experiment yielded exactly one or two foci.
- The bistable cases (two foci) are somewhat less common than the cases with a unique focus, and are characterized by values of k_R between about 3 and 5 when the velocity difference Δ was fixed at 2.

Figure 16 shows a bistable example, with the two foci and their corresponding basins of attraction. The parameter k is fixed in this and all the examples in this paper at $4 \pm i$ for the right- and left-moving beams of any given collision, respectively. The second example, shown in Fig. 17, shows that the basins are not always simply connected; a sizable island that maps to the upper focus appears within the basin of the lower focus.

5.2 A tristable example using a four-cycle

Collision cycles of length four seem to exhibit more complex behavior than those of length three, although it is difficult to draw any definite conclusions because the parameter spaces are too large to be explored exhaustively, and

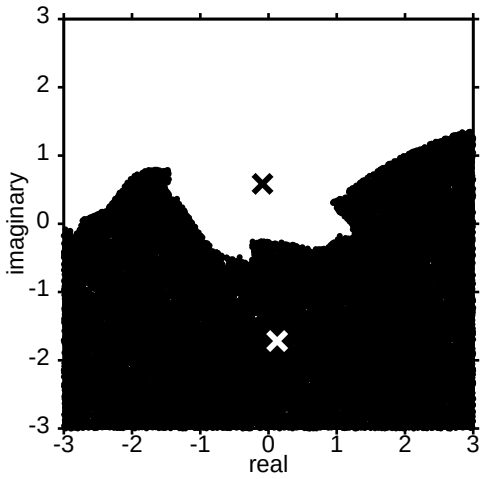

Figure 16: The two foci and their corresponding basins of attraction in the first example, which uses a cycle of three collisions. The states of the input beams are $A = -0.8 - i \cdot 0.13$, $B = 0.4 - i \cdot 0.13$, $C = 0.5 + i \cdot 1.6$; and $k = 4 \pm i$. Reprinted with permission from (Steiglitz, 2001). Copyright by the American Physical Society.

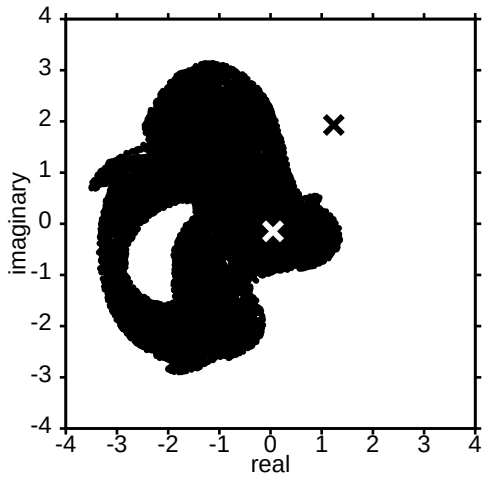

Figure 17: A second example using a cycle of three collisions, showing that the basins need not be simply connected. The states of the input beams are $A = 0.7 - i \cdot 0.3$, $B = -1.1 - i \cdot 0.5$, $C = 0.4 + i \cdot 0.81$; and $k = 4 \pm i$. Reprinted with permission from (Steiglitz, 2001). Copyright by the American Physical Society.

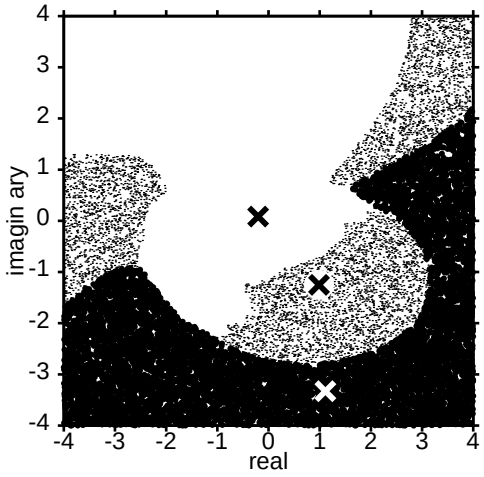

Figure 18: A case with three stable foci, for a collision cycle of length four. The states of the input beams are $A = -0.39 - i \cdot 0.45$, $B = 0.22 - i \cdot 0.25$, $C = 0.0 + i \cdot 0.25$, $D = -0.51 + i \cdot 0.48$; and $k = 4 \pm i$. Reprinted with permission from (Steiglitz, 2001). Copyright by the American Physical Society.

there is at present no theory to predict such highly nonlinear behavior. If one real degree of freedom is varied as a control parameter, we can move from bistable to tristable solutions, with a regime between in which one basin of attraction disintegrates into many small separated fragments. Clearly, this model is complex enough to exhibit many of the well-known features of nonlinear systems.

Fortunately, it is not difficult to find choices of parameters that result in very well behaved multistable solutions. For example, Fig. 18 shows such a tristable case. The smallest distance from a focus to a neighboring basin is on the order of 25% of the interfocus distance, indicating that these equilibria will be stable under reasonable noise perturbations.

5.3 Discussion

The general phenomenon discussed in this section raises many questions, both of a theoretical and practical nature. The fact that there are simple polarization-multistable cycles of collisions in a Manakov system suggests that similar situations occur in other vector systems, such as photorefractive crystals or birefringent fiber. Any vector system with the possibility of a closed cycle of soliton collisions becomes a candidate for multistability, and there is at this point really no compelling reason to restrict attention to the Manakov case, except for the fact that the explicit state-change relations make numerical study much easier.

The simplified picture we used of information traveling clockwise after we begin with a given beam a gives us stable polarization states when it converges, plus an idea of the size of their basins of attractions. It is remarkable that in all cases in our computational experience, except for borderline transitional cases in going from two to three foci in a four-cycle, this circular process converges consistently and quickly. But understanding the actual dynamics and convergence characteristics in a real material requires careful physical modeling. This modeling will depend on the nature of the medium used to approximate the Manakov system, and is left for future work. The implementation of a practical way to switch from one stable state to another is likewise critically dependent on the dynamics of soliton formation and perturbation in the particular material at hand, and must be studied with reference to a particular physical realization.

We remark also that no iron-clad conclusions can be drawn from computational experiments about the numbers of foci in any particular case, or the number possible for a given size cycle—despite the fact that we regularly used 50,000 random starting points. On the other hand, the clear cases that have been found, such as those used as examples, are very characteristic of universal behavior in other nonlinear iterated maps, and are sufficient to establish that bi- and tristability, and perhaps higher-mode multistability, is a genuine mathematical characteristic, and possibly also physically realizable. It strongly suggests experimental exploration.

We restricted discussion in this section to the simplest possible structure of a single closed cycle, with three or four collisions. The stable solutions of more complicated configurations are the subject of continuing study. A general theory that predicts this behavior is lacking, and it seems at this point unlikely to be forthcoming. This forces us to rely on numerical studies, from which, as we point out above, only certain kinds of conclusions can be drawn. We are fortunate, however, in being able to find cases that look

familiar and which are potentially useful, like the bistable three-cycles with well separated foci and simply connected basins of attraction.

It is not clear however, just what algorithms might be used to find equilibria in collision topologies with more than one cycle. It is also intriguing to speculate about how collision configurations with particular characteristics can be designed, how they can be made to interact, and how they might be controlled by pulsed beams. There is promise that when the ramifications of complexes of vector soliton collisions are more fully understood they might be useful for real computation in certain situations.

5.4 Application to noise-immune soliton computing

Any physical instantiation of a computing technology must be designed to be immune from the effects of noise buildup from logic stage to logic stage. In the familiar computers of today, built with solid-state transistors, the noise-immunity is provided by physical state restoration, so that voltage levels representing logical "0" and "1" are restored by bistable circuit mechanisms at successive logic stages. This is state restoration at the physical level.

For another example, proposed schemes for quantum computing would be impractical without some means of protecting information stored in qubits from inevitable corruption by the rest of the world. The most common method proposed for accomplishing this is error correction at the software level, state restoration at the logical level.

In the collision-based scheme for computing with Manakov solitons described in section 4, there is no protection against buildup of error from stage to stage, and some sort of logical state-restoration would be necessary in a practical realization. The bistable collision cycles of Manakov solitons described in this section, however, offer a natural computational building block for soliton computation with physical state restoration. This idea is explored in (Rand et al., 2005). Figure 19 illustrates the approach with a schematic diagram of a NAND gate, implemented with bistable cycles to represent bits. The input bits are stored in the collision cycles (1) and (2), which have output beams that can be made to collide with input beam A of cycle (3), which represents the output bit of the gate. These inputs to the gate, shown as dashed lines, change the state of beam A of the ordinarily bistable cycle (3) so that it becomes *monostable*. The state of cycle (3) is then steered to a known state. When the input beams are turned off, cycle (3) returns to its normal bistable condition, but with a known input state. Its state then evolves to one of two bits, and the whole system of three collision cycles can be engineered so that the final state of cycle (3) is the

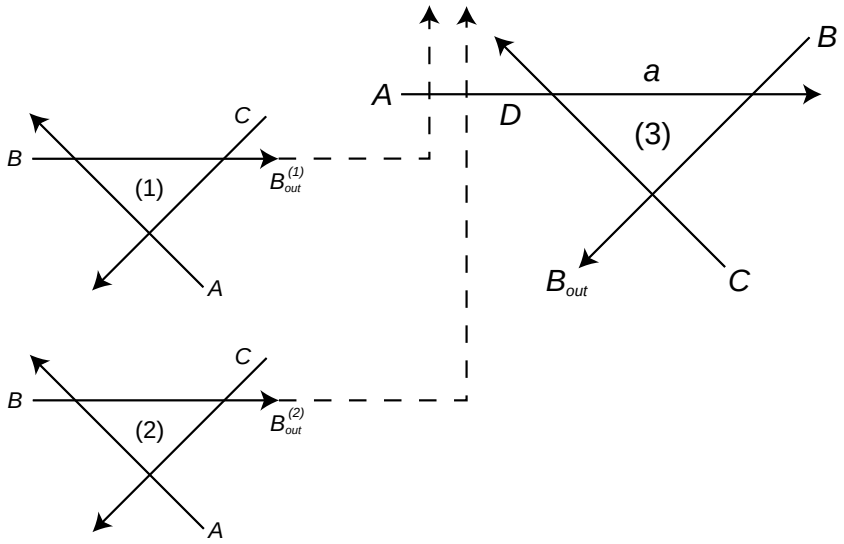

Figure 19: Schematic of NAND gate using bistable collision cycles. Reprinted with permission from (Rand et al., 2005). Copyright by Old City Publishing.

NAND of the two bits represented by input cycles (1) and (2). (See (Rand et al., 2005) for details.)

A computer based on such bistable collision cycles is closer in spirit to present-day ordinary transistor-based computers, with a natural noise-immunity and state-restoration based on physical bistability. As mentioned in the previous subsection, however, the basic bistable cycle phenomenon awaits laboratory verification, and much remains to be learned about the dynamics, and eventual speed and reliability of such systems.

6 Experiments

The computation schemes described in the previous sections obviously rely on the correct mathematical modeling of the physics proposed for realization. We next describe experiments that verify some of the required soliton phenomenology in optical fibers. Specifically, we highlight the experimental observation of temporal vector soliton propagation and collision in a birefringent optical fiber (Rand et al., 2007). This is both the first demonstration of temporal vector solitons with two mutually-incoherent component fields, and of vector soliton collisions in a Kerr nonlinear medium.

Temporal soliton pulses in optical fiber were first predicted by Hasegawa

and Tappert (1973), followed by the first experimental observation by Mollenauer et al. (1980). In subsequent work, Menyuk accounted for the birefringence in polarization maintaining fiber (PMF) and predicted that vector solitons, in which two orthogonally polarized components trap each other, are stable under the proper operating conditions (1987; 1988). For birefringent fibers, self-trapping of two orthogonally polarized pulses can occur when XPM-induced nonlinearity compensates the birefringence-induced group velocity difference, causing the pulse in the fiber's fast axis to slow down and the pulse in the slow axis to speed up. The first demonstration of temporal soliton trapping was performed in the subpicosecond regime (Islam et al., 1989), in which additional ultrashort pulse effects such as Raman scattering are present. In particular, this effect results in a red-shift that is linearly proportional to the propagation distance, as observed in a later temporal soliton trapping experiment (Nishizawa and Goto, 2002). Recently, soliton trapping in the picosecond regime was observed with equal amplitude pulses (Korolev et al., 2005). However, vector soliton propagation could not be shown, because the pulses propagated for less than 1.5 dispersion lengths. In other work, phase-locked vector solitons in a weakly birefringent fiber laser cavity with nonlinear coherent coupling between components was observed (Cundiff et al., 1999).

The theoretical model for linearly birefringent fiber is the following coupled nonlinear Schrödinger equation (CNLSE):

$$\begin{aligned} i\left(\frac{\partial A_x}{\partial z}+\beta_{1x}\frac{\partial A_x}{\partial t}\right)-\frac{\beta_2}{2}\frac{\partial^2 A_x}{\partial t^2}+\gamma\left(|A_x|^2+\frac{2}{3}|A_y|^2\right)A_x=0,\\ i\left(\frac{\partial A_y}{\partial z}+\beta_{1y}\frac{\partial A_y}{\partial t}\right)-\frac{\beta_2}{2}\frac{\partial^2 A_y}{\partial t^2}+\gamma\left(|A_y|^2+\frac{2}{3}|A_x|^2\right)A_y=0, \end{aligned} \tag{10}$$

where t is the local time of the pulse, z is propagation distance along the fiber, and $A_{x,y}$ is the slowly varying pulse envelope for each polarization component. The parameter $\beta_{1x,y}$ is the group velocity associated with each fiber axis, and β_2 represents the group velocity dispersion, assumed equal for both polarizations. In addition, we neglect higher order dispersion and assume a lossless medium with an instantaneous electronic response, valid for picosecond pulses propagating in optical fiber.

The last two terms of Eqs. (10) account for the nonlinearity due to SPM and XPM, respectively. In linearly birefringent optical fiber, a ratio of 2/3 exists between these two terms. When this ratio equals unity, the CNLSE becomes the integrable Manakov system of Eqs. (4). On the other hand, solutions of Eqs. (10) are, strictly speaking, solitary waves, not solitons. However, it was found in (Yang, 1997) that the family of symmetric,

single-humped (fundamental or first-order) solutions, to which the current investigation in this section belongs, are all stable. Higher-order solitons, characterized by multiple humps, are unstable. Furthermore, it was shown in (Yang, 1999) that collisions of solitary waves in Eqs. (10) can be described by application of perturbation theory to the integrable Manakov equations, indicating the similarities between the characteristics of these two systems.

6.1 Experimental setup and design

The experimental setup is shown in Fig. 20. We synchronized two actively mode-locked erbium-doped fiber lasers (EDFLs)—EDFL1 at 1.25 GHz repetition rate, and EDFL2 at 5 GHz. EDFL2 was modulated to match with the lower repetition rate of EDFL1. Each pulse train, consisting of 2 ps pulses, was amplified in an erbium-doped fiber amplifier (EDFA) and combined in a fiber coupler. To align polarizations, a polarization loop controller (PLC) was used in one arm, and a tunable delay line (TDL) was employed to temporally align the pulses for collision. Once combined, both pulse trains passed through a linear polarizer (LP) and a half-wave plate to control the input polarization to the PMF. Approximately 2 m of high birefringence (HB) PMF preceded the specially designed 500 m of low birefringence (LB) PMF used to propagate vector solitons. Although this short length of HB-PMF will introduce some pulse splitting (on the order of 2-3 ps), the birefringent axes of the HB- and LB-PMF were swapped in order to counteract this effect. Each component of the vector soliton was then split at a polarization beam splitter, followed by an optical spectrum analyzer (OSA) for measurement.

The design of the LB-PMF required careful control over three characteristic length scales: the (polarization) beat length, dispersion length $L_{\rm d}$, and nonlinear length $L_{\rm nl}$. A beat length $L_{\rm b} = \lambda/\Delta n = 50$ cm was chosen at a wavelength of 1550 nm, where Δn is the fiber birefringence. According to the approximate stability criterion of (Cao and McKinstrie, 1993), this choice allows stable propagation of picosecond vector solitons. By avoiding the subpicosecond regime, ultrashort pulse effects such as intrapulse Raman scattering will not be present. The dispersion $D = 2\pi c\beta_2/\lambda^2 = 16$ ps/km nm and $L_{\rm d} = 2T_0^2/|\beta_2| \approx 70$ m, where $T_0 = T_{\rm FWHM}/1.763$ is a characteristic pulse width related to the full width at half maximum (FWHM) pulse width. Since $L_{\rm d} \gg L_{\rm b}$, degenerate four-wave mixing due to coherent coupling between the two polarization components can be neglected (Menyuk, 1989). Furthermore, the total propagation distance is greater than 7 dispersion lengths.

Polarization instability, in which the fast axis component is unstable,

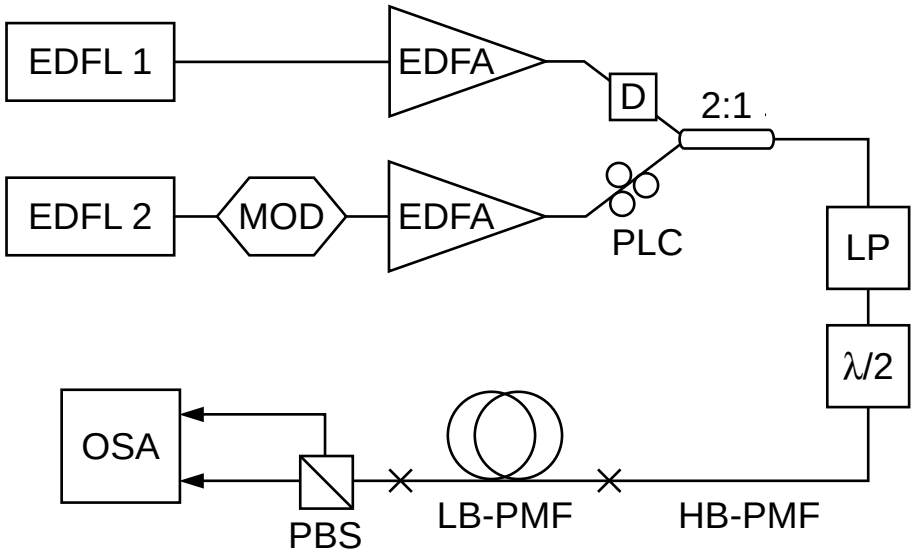

Figure 20: Experimental setup. EDFL: Erbium-doped fiber laser; EDFA: Erbium-doped fiber amplifier; MOD: modulator; D: tunable delay line; PLC: polarization loop controller; 2:1: fiber coupler; LP: linear polarizer; $\lambda/2$: half-wave plate; HB-PMF and LB-PMF: high and low birefringence polarization maintaining fiber; PBS: polarization beam splitter; OSA: optical spectrum analyzer. Reprinted with permission from (Rand et al., 2007). Copyright by the American Physical Society.

occurs when $L_{\rm nl} = (\gamma P)^{-1}$ is of the same order of magnitude or smaller than $L_{\rm b}$, as observed in (Barad and Silberberg, 1997). The nonlinearity parameter $\gamma = 2\pi n_2/\lambda A_{\rm eff} = 1.3$ (km W)$^{-1}$, with Kerr nonlinearity coefficient $n_2 = 2.6 \times 10^{-20}$ m^2/W and measured effective mode area $A_{\rm eff} = 83$ μm^2. In the LB-PMF, the fundamental vector soliton power $P \approx 14$ W, thus $L_{\rm nl} = 55$ m $\gg L_{\rm b}$, mitigating the effect of polarization instability.

6.2 Vector soliton propagation

We first studied propagation of vector solitons using both lasers independently. The wavelength shift for each component is shown in Fig. 21(a) as a function of the input polarization angle ϕ, controlled through the half-wave plate. Due to the anomalous dispersion of the fiber at this wavelength, the component in the slow (fast) axis will shift to shorter (longer) wavelengths to compensate the birefringence. The total amount of wavelength shift between components $\Delta\lambda_{xy} = \Delta\beta_1/D = 0.64$ nm, where $\Delta\beta_1 = |\beta_{1x} - \beta_{1y}| = 10.3$ ps/km is the birefringence-induced group velocity difference and dispersion $D = 2\pi c\beta_2/\lambda^2 = 16$ ps/km nm.

As ϕ approaches 0° (90°), the vector soliton approaches the scalar soliton limit, and the fast (slow) axis does not shift in wavelength, as expected. At $\phi = 45°$, a symmetric shift results. For unequal amplitude solitons, the smaller component shifts more in wavelength than the larger component, because the former experiences more XPM. Numerical simulations of Eqs. (10), given by the dashed lines of Fig. 21(a), agree very well with the experimental results. Also shown in Fig. 21 are two cases, $\phi = 45°$ and 37°, as well as the numerical prediction. The experimental spectra show some oscillatory features at 5 GHz, which are a modulation of the EDFL2 repetition rate on the optical spectrum. A sample input pulse spectrum from EDFL1 is shown in the inset of Fig. 21, which shows no modulation due to the limited resolution of the OSA. Vector solitons from both lasers produced similar results. In this and all subsequent plots in this section, the slow and fast axis components are depicted by solid and dashed lines, respectively.

As the two component amplitudes become more unequal, satellite peaks become more pronounced in the smaller component. These features are also present in the simulations, but are not as dominant (cf. Figs. 21(d) and (e)). We attribute this to the input pulse, which is calibrated for the $\phi = 45°$ case, because the power threshold for vector soliton formation in this case is largest due to the 2/3 factor between SPM and XPM nonlinear terms in the CNLSE. As the input is rotated towards unequal components, there will be extra power in the input pulse, which will radiate in the form

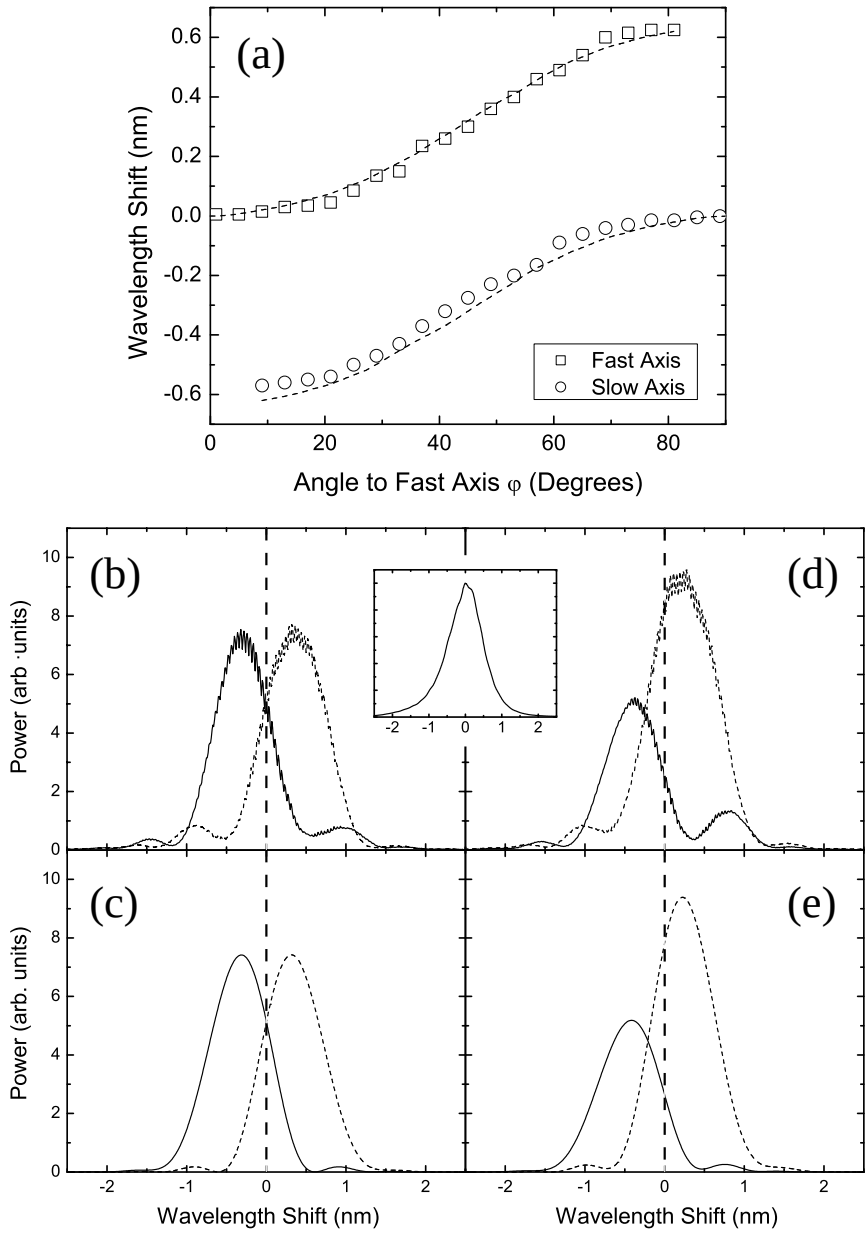

Figure 21: Arbitrary-amplitude vector soliton propagation. (a) Wavelength shift vs. angle to fast axis ϕ, numerical curves given by dashed lines; (b) and (d) experimental results for $\phi = 45°$ and 37° with EDFL2, respectively. Inset: input spectrum for EDFL1; (c) and (e) corresponding numerical simulations of $\phi = 45°$ and 37°, respectively. The slow and fast axis components are depicted by solid and dashed lines, respectively. Reprinted with permission from (Rand et al., 2007). Copyright by the American Physical Society.

of dispersive waves as the vector soliton forms. Due to the nature of this system, these dispersive waves can be nonlinearly trapped, giving rise to the satellite features in the optical spectra. This effect is not as prevalent in the simulations because the threshold was numerically determined at each input angle ϕ.

6.3 Vector soliton collision

To prepare the experiment for a collision, we operated both lasers simultaneously, detuned in wavelength to allow for dispersion-induced walkoff, and adjusted the delay line in such a way that the collision occurred halfway down the fiber. We define a collision length $L_{\text{coll}} = 2T_{\text{FWHM}}/D\Delta\lambda$, where $\Delta\lambda$ is the wavelength separation between the two vector solitons. For our setup, $\Delta\lambda = 3$ nm, and $L_{\text{coll}} = 83.3$ m. An asymptotic theory of soliton collisions, in which a full collision takes place, requires at least 5 collision lengths. The total fiber length in this experiment is equal to 6 collision lengths, long enough to ensure sufficient separation of solitons before and after collision. In this way, results of our experiments can be compared to the asymptotic theory, even though full numerical simulations will be shown for comparison. To quantify our results, we introduce a quantity $R \equiv \tan^2\phi$, defined as the amplitude ratio between the slow and fast components.

Recall that in Section 3, we introduced the Manakov equations (Eqs. (4)), and described collision-induced transformations of the polarization state of the soliton, which come about due to the asymptotic analysis of the soliton collision. The polarization state is the ratio between the two components $\rho \equiv A_x/A_y = \cot\phi\exp(i\Delta\theta)$, and is therefore a function of the polarization angle ϕ and the relative phase $\Delta\theta$ between the two components. In the context of the experiments described in this chapter, these state transformations (Eqs. (5) and (7)) predict that the resulting energy exchange will be a function of amplitude ratios $R_{1,2}$, wavelength separation $\Delta\lambda$, and the relative phase $\Delta\theta_{1,2}$ between the two components of each soliton, where soliton 1 (2) is the shorter (longer) wavelength soliton.

A word of caution is in order at this point. An interesting consequence of the 2/3 ratio between SPM and XPM, which sets the birefringent fiber model apart from the Manakov model, is the relative phase between the two components. For the Manakov soliton, each component 'feels' the same amount of total nonlinearity, because the strengths of both SPM and XPM are equal. Therefore, regardless of the polarization angle, the amount of total nonlinear phase shift for each component is the same (even though the contributions of SPM and XPM phase shifts are in general not equal).

As a result, the relative phase between the two components stays constant during propagation, as does the polarization state. This is *not* the case for vector solitons in birefringent fiber. For the case of equal amplitudes, each component does experience the same amount of nonlinear phase shift, and therefore the polarization state is constant as a function of propagation distance. However, for arbitrary (unequal) amplitudes, the total phase shift for each component will be different. Consequently, the relative phase will change *linearly* as a function of propagation distance, and the polarization state will not be constant. As a result, the collision-induced change in polarization state, while being a function of the amplitude ratios $R_{1,2}$ and wavelength separation $\Delta\lambda$, will also depend upon the collision position due to the propagation dependence of the relative phase $\Delta\theta_{1,2}(z)$. To bypass this complication, we ensure that all collisions occur at the same spatial point in the fiber.

Because only one half-wave plate is used in our experiment (see Fig. 20), it was not possible to prepare each vector soliton individually with an arbitrary R. In addition, due to the wavelength dependence of the half-wave plate, it was not possible to adjust $\Delta\lambda$ without affecting R.

First, we investigated the phase dependence of the collision. This was done by changing the length of the HB-PMF entering the LB-PMF, while keeping R and $\Delta\lambda$ constant. As a result, we could change $\Delta\theta_{1,2}$ due to the birefringence of the HB-PMF. Approximately 0.5 m of HB-PMF was added to ensure that the total amount of temporal pulse splitting did not affect the vector soliton formation. The results are shown in Fig. 22, where Figs. 22(a-c) and (d-f) correspond to the short and long HB-PMFs, respectively. Figs. 22(a) and (d) show the two vector solitons, which propagate independently when no collision occurs; as expected, the two results are similar because the OSA measurement does not depend on $\Delta\theta_{1,2}$. The result of the collision is depicted in Figs. 22(b) and (e), along with the corresponding simulation results in Figs. 22(c) and (f).

In both of these collisions, an energy exchange between components occurs, and two important relations are satisfied: the total energy in each soliton and in each component is conserved. It can be seen that when one component in a soliton increases as a result of the collision, the other component decreases, with the opposite exchange in the second soliton. The difference between these two collisions is dramatic, in that the energy redistributes in opposite directions. For the simulations, idealized sech pulses for each component were used as initial conditions, and propagation was modeled without accounting for losses. The experimental amplitude ratio was used, and (without loss of generality (Manakov, 1973; Radhakrishnan

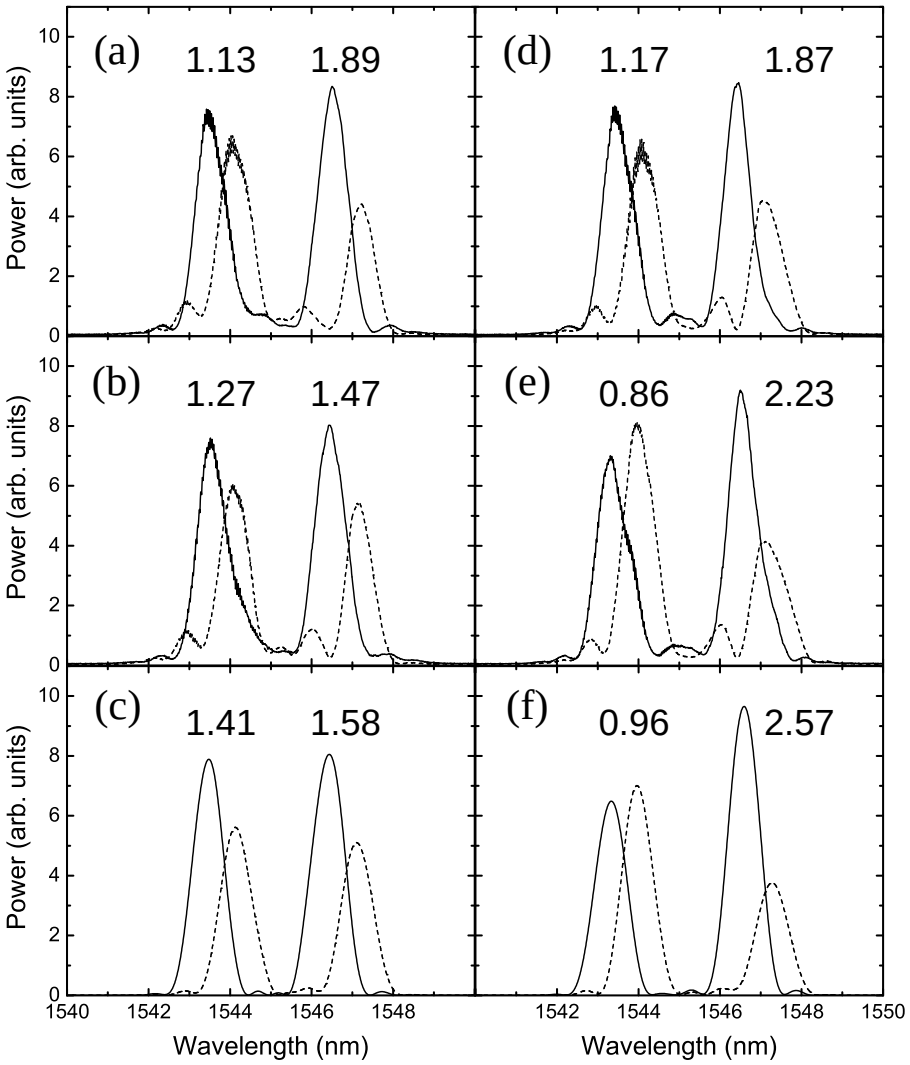

Figure 22: Demonstration of phase-dependent energy-exchanging collisions. (a-c) Short HB-PMF; (d-f) long HB-PMF; (a, d) experiment, without collision; (b, e) experiment, with collision; (c, f) simulated collision result with (c) $\Delta\theta_2 = 90°$ and (f) $\Delta\theta_2 = 50°$. Values of slow-fast amplitude ratio R are given above each soliton. The slow and fast axis components are depicted by solid and dashed lines, respectively. Reprinted with permission from (Rand et al., 2007). Copyright by the American Physical Society.

et al., 1997; Jakubowski et al., 1998)) $\Delta\theta_2$ was varied while $\Delta\theta_1 = 0$. Best fits gave $\Delta\theta_2 = 90°$ (Fig. 22(c)) and $50°$ (Fig. 22(f)). Despite the model approximations, experimental and numerical results all agree to within 15%.

In the second set of results (Fig. 23), we changed R while keeping all other parameters constant. More specifically, we used the short HB-PMF, with initial phase difference $\Delta\theta_2 = 90°$, and changed the amplitude ratio. In agreement with theoretical predictions, the same direction of energy exchange is observed as in Figs. 22(a-c).

6.4 Spatial soliton collisions

We mention here analogous experiments with spatial solitons in photorefractive media by Anastassiou et al. In (Anastassiou et al., 1999), it is shown that energy is transferred in a collision of vector spatial solitons in a way consistent with the predictions for the Manakov system (although the medium is a saturable one, and only approximates the Kerr nonlinearity). The experiment in (Anastassiou et al., 2001) goes one step farther, showing that one soliton can be used as an intermediary to transfer energy from a second soliton to a third. We thus are now at a point where the ability of both temporal and spatial vector solitons to process information for computation has been demonstrated.

7 Future Directions

This article discussed computing with solitons, and attempted to address the subject from basic physical principles to applications. Although the nonlinearity of fibers is very weak, the ultralow loss and tight modal confinement make them technologically attractive. By no means, however, are they the only potential material for soliton-based information processing. Others include photorefractive crystals, semiconductor waveguides, quadratic media, and Bose-Einstein condensates, while future materials research may provide new candidate systems.

From a computing perspective, scalar soliton collisions are insufficient. Although measurable phase and position shifts do occur, these phenomena cannot be cascaded to affect future soliton collisions and therefore cannot transfer information from one collision to the next. Meaningful computation using soliton collisions requires a new degree of freedom; that is, a new component. Collisions of vector solitons display interesting energy-exchanging effects between components, which can be exploited for arbitrary computation and bistability.

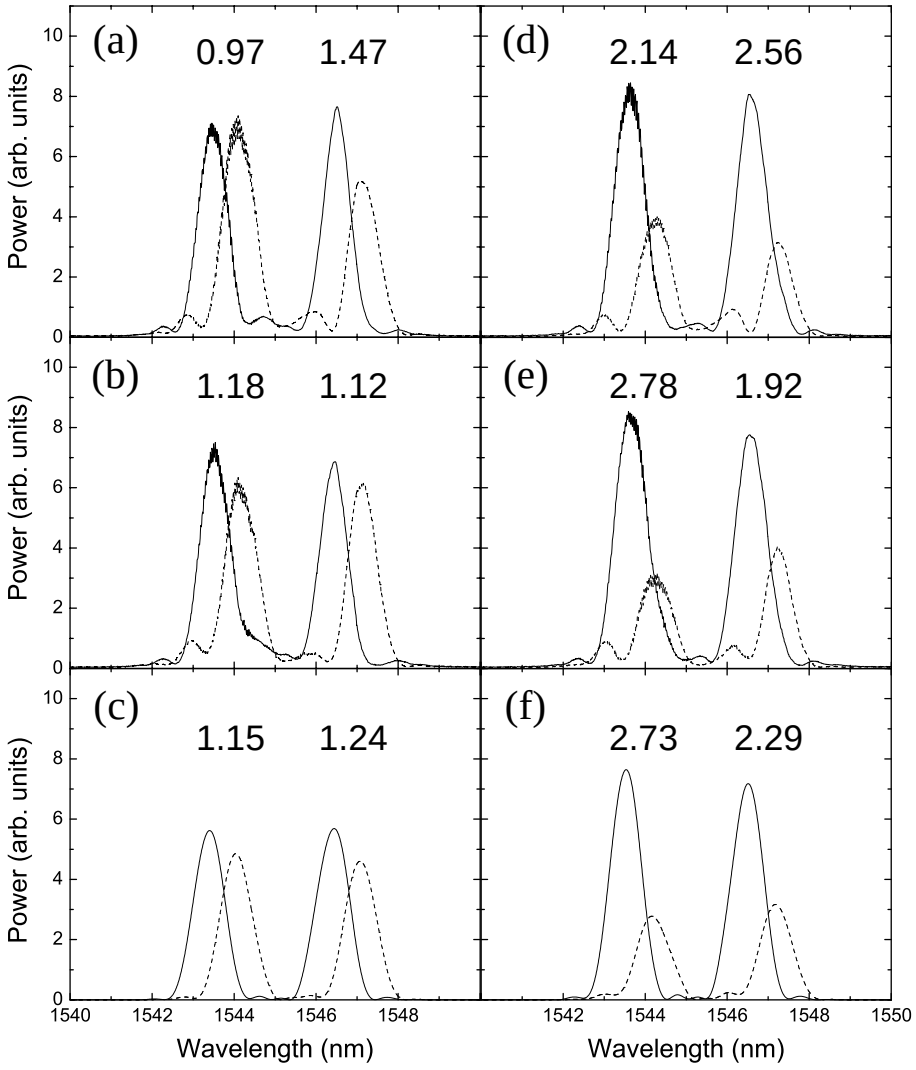

Figure 23: Additional energy-exchanging collisions. (a, d) Experiment, without collision; (b, e) experiment, with collision; (c, f) simulated collision result, using $\Delta\theta_2 = 90^\circ$ inferred from the experiment of Fig. 22. Values of slow-fast amplitude ratio R are given above each soliton. The slow and fast axis components are depicted by solid and dashed lines, respectively. Reprinted with permission from (Rand et al., 2007). Copyright by the American Physical Society.

The vector soliton experiments of section 6 were proof-of-principle ones. The first follow-up experiments with temporal vector solitons in birefringent fiber can be directed towards a full characterization of the collision process. This can be done fairly simply using the experimental setup of Fig. 20 updated in such a way as to allow independent control of two vector soliton inputs. This would involve separate polarizers and half-waveplates, followed by a polarization preserving fiber coupler.

Cascaded collisions of temporal solitons also await experimental study. As demonstrated in photorefractive crystals with a saturable nonlinearity (Anastassiou et al., 2001), one can show that information can be passed from one collision to the next. Beyond a first demonstration of two collisions is the prospect of setting up a multi-collision feedback cycle. Discussed in section 5, these collision cycles can be bistable and lead to interesting applications in computation.

Furthermore, the recent work of Ablowitz et al. (2006) shows theoretically that the useful energy-redistribution properties of vector soliton collisions extend perfectly to the semi-discrete case: that is, to the case where space is discretized, but time remains continuous. This models, for example, propagation in an array of coupled nonlinear waveguides (Christodoulides and Joseph, 1988). The work suggests alternative physical implementations for soliton switching or computing, and also hints that the phenomenon of soliton information processing is a very general one.

References

Ablowitz, M. J., Prinari, B., and Trubatch, A. D.: 2004, *Inverse Problems* **20(4)**, 1217

Ablowitz, M. J., Prinari, B., and Trubatch, A. D.: 2006, *Studies in Appl. Math.* **116**, 97

Agrawal, G. P.: 2001, *Nonlinear Fiber Optics*, Academic Press, 3rd edition

Anastassiou, C., Fleischer, J. W., Carmon, T., Segev, M., and Steiglitz, K.: 2001, *Opt. Lett.* **26(19)**, 1498

Anastassiou, C., Segev, M., Steiglitz, K., Giordmaine, J. A., Mitchell, M., Shih, M. F., Lan, S., and Martin, J.: 1999, *Phys. Rev. Lett.* **83(12)**, 2332

Barad, Y. and Silberberg, Y.: 1997, *Phys. Rev. Lett.* **78**, 3290

Berlekamp, E. R., Conway, J. H., and Guy, R. K.: 1982, *Winning ways for your mathematical plays. Vol. 2*, Academic Press Inc. [Harcourt Brace Jovanovich Publishers], London

Cao, X. D. and McKinstrie, C. J.: 1993, *J. Opt. Soc. Am. B* **10**, 1202
Chen, Z. G., Segev, M., Coskun, T. H., and Christodoulides, D. N.: 1996, *Opt. Lett.* **21(18)**, 1436
Christodoulides, D. N. and Joseph, R. I.: 1988, **13**, 794
Christodoulides, D. N., Singh, S. R., Carvalho, M. I., and Segev, M.: 1996, *Appl. Phys. Lett.* **68(13)**, 1763
Cundiff, S. T., Collings, B. C., Akhmediev, N. N., Soto-Crespo, J. M., Bergman, K., and Knox, W. H.: 1999, *Phys. Rev. Lett.* **82**, 3988
Fredkin, E. and Toffoli, T.: 1982, *Int. J. Theor. Phys.* **21(3/4)**, 219
Hasegawa, A. and Tappert, F.: 1973, *Appl. Phys. Lett.* **23(3)**, 142
Islam, M. N., Poole, C. D., and Gordon, J. P.: 1989, *Opt. Lett.* **14**, 1011
Jakubowski, M. H., Steiglitz, K., and Squier, R.: 1998, *Phys. Rev. E* **58(5)**, 6752
Kang, J. U., Stegeman, G. I., Aitchison, J. S., and Akhmediev, N.: 1996, *Phys. Rev. Lett.* **76(20)**, 3699
Korolev, A. E., Nazarov, V. N., Nolan, D. A., and Truesdale, C. M.: 2005, *Opt. Lett.* **14**, 132
Manakov, S. V.: 1973, *Zh. Eksp. Teor. Fiz.* **65(2)**, 505, [Sov. Phys. JETP **38**, 248 (1974)]
Mano, M. M.: 1972, *Computer Logic Design*, Prentice-Hall, Englewood Cliffs, NJ
Menyuk, C. R.: 1987, *Opt. Lett.* **12**, 614
Menyuk, C. R.: 1988, *J. Opt. Soc. Am. B* **5**, 392
Menyuk, C. R.: 1989, *IEEE J. Quant. Elect.* **25(12)**, 2674
Mollenauer, L. F., Stolen, R. H., and Gordon, J. P.: 1980, *Phys. Rev. Lett.* **45(13)**, 1095
Nishizawa, N. and Goto, T.: 2002, **10**, 256
Radhakrishnan, R., Lakshmanan, M., and Hietarinta, J.: 1997, *Phys. Rev. E* **56(2)**, 2213
Rand, D., Glesk, I., Brès, C.-S., Nolan, D. A., Chen, X., Koh, J., Fleischer, J. W., Steiglitz, K., and Prucnal, P. R.: 2007, *Phys. Rev. Lett.* **98(5)**, 053902
Rand, D., Steiglitz, K., and Prucnal, P. R.: 2005, *Int. J. of Unconv. Comp.* **1**, 31
Russell, J. S.: 1844, in *Report of the 14th meeting of the British Association for the Advancement of Science*, pp 331–390
Shih, M. F. and Segev, M.: 1996, *Opt. Lett.* **21(19)**, 1538
Shor, P. W.: 1994, in *35th Annual Symposium on Foundations of Computer Science*, pp 20–22, IEEE Press
Squier, R. K. and Steiglitz, K.: 1993, *Complex Systems* **7**, 297

Steblina, V. V., Buryak, A. V., Sammut, R. A., Zhou, D. Y., Segev, M., and Prucnal, P.: 2000, *J. Opt. Soc. Am. B* **17(12)**, 2026
Steiglitz, K.: 2000, *Phys. Rev. E* **63(1)**, 016608
Steiglitz, K.: 2001, *Phys. Rev. E* **63(4)**, 046607
Yang, J.: 1997, *Physica D* **108**, 92
Yang, J.: 1999, *Phys. Rev. E* **59(2)**, 2393
Zakharov, V. E. and Shabat, A. B.: 1971, *Zh. Eksp. Teor. Fiz.* **61(1)**, 118, [Sov. Phys. JETP **34**, 62 (1972)]